

MAPTR: STRUCTURED MODELING AND LEARNING FOR ONLINE VECTORIZED HD MAP CONSTRUCTION

Bencheng Liao^{1,2,3*} **Shaoyu Chen**^{1,3*} **Xinggang Wang**^{1†}
Tianheng Cheng^{1,3} **Qian Zhang**³ **Wenyu Liu**¹ **Chang Huang**³

¹ School of EIC, Huazhong University of Science & Technology

² Institute of Artificial Intelligence, Huazhong University of Science & Technology

³ Horizon Robotics

{bcliao, shaoyuchen, xgwang, thch, liuwu}@hust.edu.cn

{qian01.zhang, chang.huang}@horizon.ai

ABSTRACT

We present MapTR, a structured end-to-end framework for efficient online vectorized HD map construction. We propose a unified permutation-based modeling approach, *i.e.*, modeling map element as a point set with a group of equivalent permutations, which avoids the definition ambiguity of map element and eases learning. We adopt a hierarchical query embedding scheme to flexibly encode structured map information and perform hierarchical bipartite matching for map element learning. MapTR achieves the best performance and efficiency among existing vectorized map construction approaches on nuScenes dataset. In particular, MapTR-nano runs at real-time inference speed (25.1 FPS) on RTX 3090, 8× faster than the existing state-of-the-art camera-based method while achieving 3.3 higher mAP. MapTR-tiny significantly outperforms the existing state-of-the-art multi-modality method by 13.5 mAP while being faster. Qualitative results show that MapTR maintains stable and robust map construction quality in complex and various driving scenes. Abundant demos are available at <https://github.com/hustvl/MapTR> to prove the effectiveness in real-world scenarios. MapTR is of great application value in autonomous driving. Code will be released for facilitating further research and application.

1 INTRODUCTION

High-definition (HD) map contains rich semantic information of road topology and traffic rules, serving as a fundamental and indispensable component of self-driving system. Conventionally HD map is constructed offline with SLAM-based methods (Zhang & Singh, 2014; Shan & Englot, 2018; Shan et al., 2020), incurring high maintaining cost and scalability issue. Recently, online HD map construction has attracted ever-increasing interests, which constructs map around ego-vehicle at runtime with onboard sensors, getting rid of offline human efforts.

Lane detection can be regarded as a sub task of HD map construction. Related works (Chen et al., 2022a; Liu et al., 2021a; Can et al., 2021) leverage priors to perceive open-shape lanes based on front-view images. They are restricted to single-view perception and can not cope with other map elements with dynamic shapes. With the development of bird’s eye view (BEV) representation learning, recent works (Chen et al., 2022b; Zhou & Krähenbühl, 2022; Hu et al., 2021; Li et al., 2022c) predict rasterized map by performing BEV semantic segmentation. However, the rasterized map lacks vectorized instance-level information, such as the lane structure, which is important for the downstream tasks (*e.g.*, motion prediction and planning). To construct vectorized HD map, HDMapNet (Li et al., 2022a) groups pixel-wise segmentation results in the post-processing, which is complicated and time-consuming. To avoid the post-processing, VectorMapNet (Liu et al., 2022a)

*Equal contribution.

†Corresponding author.

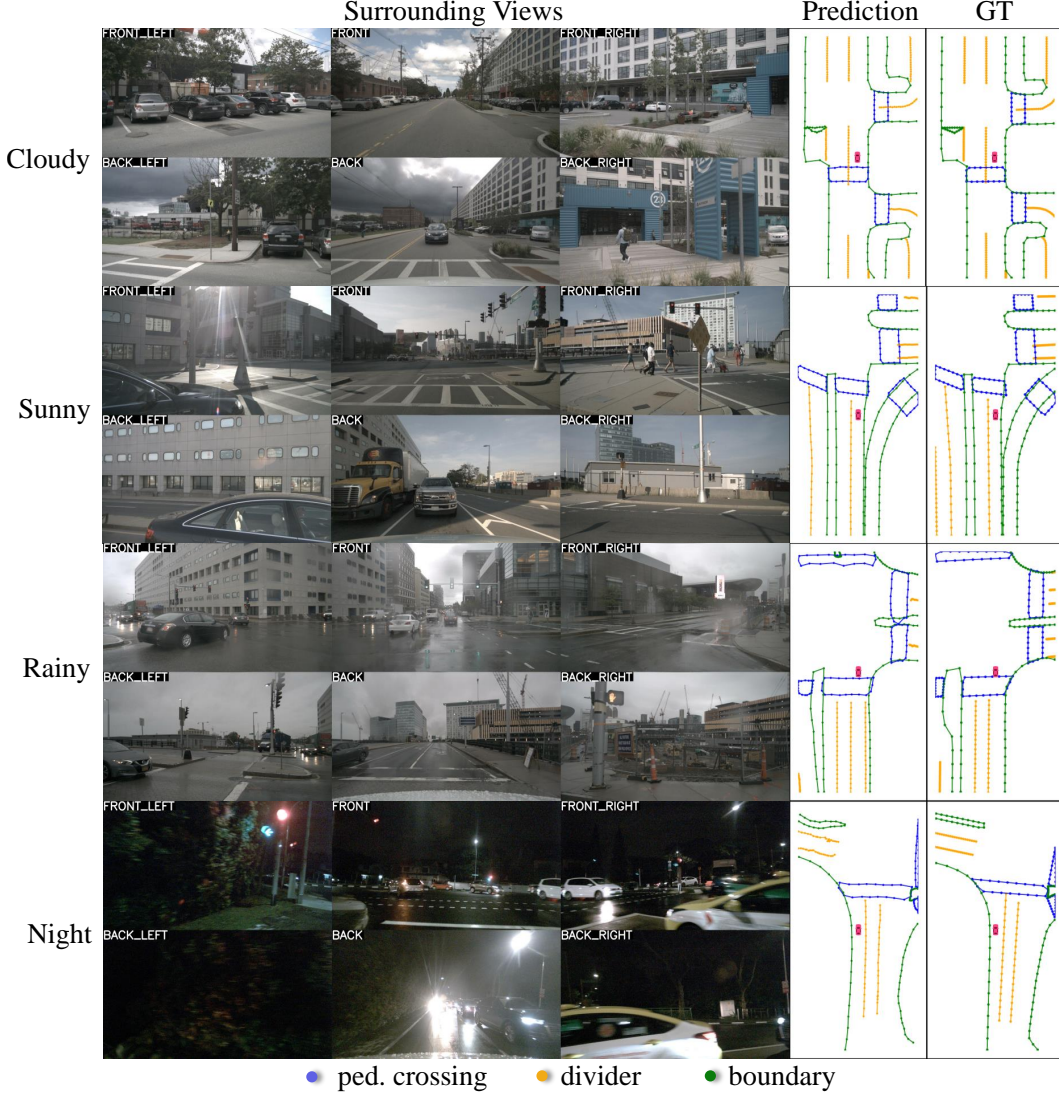


Figure 1. MapTR maintains stable and robust map construction quality in complex and various driving scenes.

represents each map element as a directed polyline, and utilizes auto-regressive decoder to predict the next point of the polyline sequentially. Despite its good performance, VectorMapNet has its own issues: (1) Representing map elements with directed polylines and sequentially predicting points incur definition ambiguity (refer to Fig. 2). Such modeling requires that all map elements have an explicit definition of start point and direction. However, for closed-shape elements (*e.g.*, pedestrian crossing) and some line elements (*e.g.*, divider between opposite lanes), there is no reasonable criterion to define the start point and direction. (2) VectorMapNet predicts points in a recurrent manner and adopts a cascaded coarse-to-fine framework, leading to longer inference time and limited scalability to the real-time scenario. (3) The recurrent nature of auto-regressive decoder incurs the problem of accumulated error, requiring much longer training epochs for convergence.

In this work, we present **Map TR**ansformer (MapTR), for efficient online vectorized HD map construction. We propose a unified permutation-based modeling approach for various kinds of map elements (both closed and open shapes), *i.e.*, modeling map element as a point set with a group of equivalent permutations. The point set determines the position of the map element. And the permutation group includes all the possible organization sequences of the point set corresponding to the same geometrical shape, avoiding the definition ambiguity of map element.

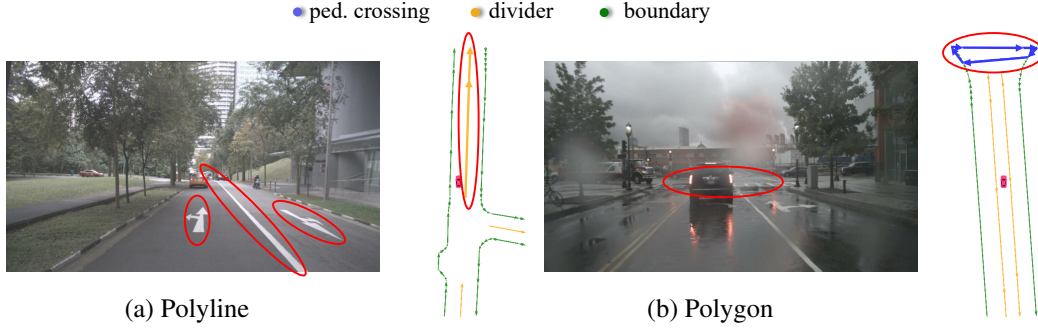


Figure 2. Typical cases for illustrating the definition ambiguity of map element about start point and direction. (a) Polyline: for the lane divider between two opposite lanes, defining its direction is difficult. Both endpoints of the lane divider can be regarded as the start point and the point set can be organized in two directions. (b) Polygon: for the pedestrian crossing, each point of the polygon can be regarded as the start point, and the polygon can be connected in two opposite directions (counter-clockwise and clockwise).

Based on permutation-based modeling, MapTR builds a structured framework for map learning. MapTR treats online vectorized HD map construction as a parallel regression problem. Hierarchical query embeddings are adopted to flexibly encode instance-level and point-level information. All instances and all points of instance are simultaneously predicted with a unified Transformer structure. And MapTR formulates the training pipeline as a hierarchical set prediction task. We perform hierarchical bipartite matching to assign instances and points in turn.

MapTR achieves the best performance and efficiency among existing vectorized map construction approaches on nuScenes (Caesar et al., 2020) dataset. In particular, MapTR-nano runs at real-time inference speed (25.1 FPS) on RTX 3090, $8\times$ faster than the existing state-of-the-art camera-based method while achieving 3.3 higher mAP. MapTR-tiny significantly outperforms the existing state-of-the-art multi-modality method by 13.5 mAP while being faster. As the visualization shows (Fig. 1), MapTR maintains stable and robust map construction quality in complex and various driving scenes. It is of great application value in autonomous driving.

Our contributions can be summarized as follows:

- We propose a unified permutation-based modeling approach for map elements, *i.e.*, modeling map element as a point set with a group of equivalent permutations, which avoids the definition ambiguity of map element and eases learning.
- Based on the novel modeling, we present MapTR, a structured end-to-end framework for efficient online vectorized HD map construction. We introduce a hierarchical query embedding scheme to flexibly encode instance-level and point-level information and perform hierarchical bipartite matching for map element learning.
- MapTR is the **first real-time** and **SOTA** vectorized HD map construction approach with stable and robust performance in complex and various driving scenes. It is of great application value in autonomous driving.

2 MAPTR

2.1 PERMUTATION-BASED MODELING

MapTR aims at modeling and learning the HD map in a structured manner. HD map is a collection of static map elements, including pedestrian crossing, lane divider, road boundary, *etc.* For structured modeling, MapTR geometrically abstracts map elements as closed shape (like pedestrian crossing) and open shape (like lane dividers). Through sampling points sequentially along the shape boundary, closed-shape element is discretized into polygon while open-shape element is discretized into polyline.

Preliminarily, both polygon and polyline can be represented as an ordered point set $V^F = [v_0, v_1, \dots, v_{N_v-1}]$ (see Fig. 3 (Vanilla)). N_v denotes the number of points. However, the per-

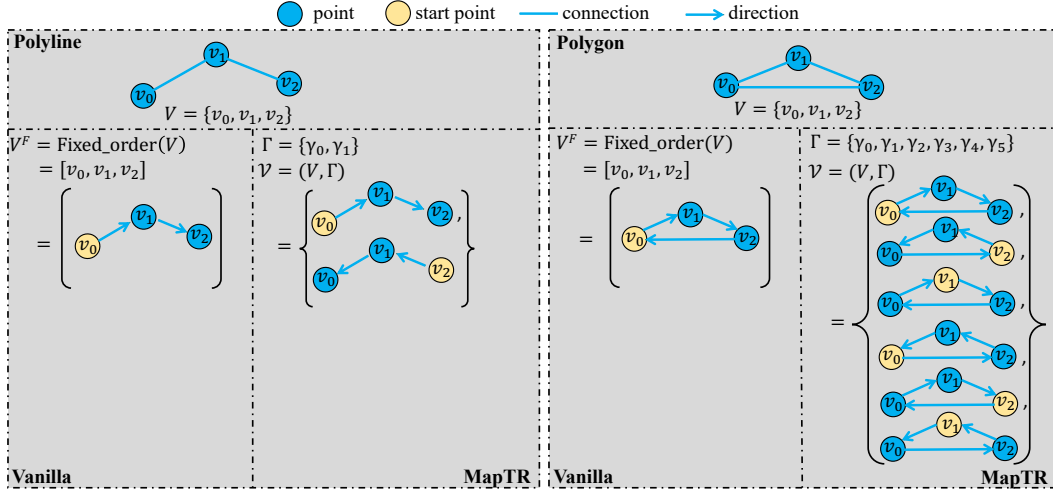


Figure 3. Illustration of permutation-based modeling of MapTR. Map elements are geometrically abstracted and discretized into polylines and polygons. MapTR models each map element with (V, Γ) (a point set V and a group of equivalent permutations Γ), avoiding the definition ambiguity and easing learning.

mutation of the point set is not explicitly defined and not unique. There exist many equivalent permutations for polygon and polyline. For example, as illustrated in Fig. 2 (a), for the lane divider (polyline) between two opposite lanes, defining its direction is difficult. Both endpoints of the lane divider can be regarded as the start point and the point set can be organized in two directions. In Fig. 2 (b), for the pedestrian crossing (polygon), the point set can be organized in two opposite directions (counter-clockwise and clockwise). And circularly changing the permutation of point set has no influence on the geometrical shape of the polygon. In a word, imposing a unique permutation to the point set leads to definition ambiguity.

To bridge this gap, MapTR models each map element with $\mathcal{V} = (V, \Gamma)$. $V = \{v_j\}_{j=0}^{N_v-1}$ denotes the point set of the map element (N_v is the number of points). $\Gamma = \{\gamma_k\}$ denotes a group of equivalent permutations of the point set V , covering all the possible organization sequences.

Specifically, for polyline element (see Fig. 3 (left)), Γ includes 2 kinds of equivalent permutations, *i.e.*,

$$\Gamma_{\text{polyline}} = \{\gamma_0, \gamma_1\} \begin{cases} \gamma_0(j) = j \mod N_v, \\ \gamma_1(j) = (N_v - 1) - j \mod N_v. \end{cases} \quad (1)$$

For polygon element (see Fig. 3 (right)), Γ includes $2 \times N_v$ kinds of equivalent permutations, *i.e.*,

$$\Gamma_{\text{polygon}} = \{\gamma_0, \dots, \gamma_{2 \times N_v - 1}\} \begin{cases} \gamma_0(j) = j \mod N_v, \\ \gamma_1(j) = (N_v - 1) - j \mod N_v, \\ \gamma_2(j) = (j + 1) \mod N_v, \\ \gamma_3(j) = (N_v - 1) - (j + 1) \mod N_v, \\ \dots \\ \gamma_{2 \times N_v - 2}(j) = (j + N_v - 1) \mod N_v, \\ \gamma_{2 \times N_v - 1}(j) = (N_v - 1) - (j + N_v - 1) \mod N_v. \end{cases} \quad (2)$$

By introducing the conception of equivalent permutations, MapTR models map elements in a unified manner and avoids the ambiguity problem. Based on such modeling, MapTR further introduces hierarchical bipartite matching (see Sec. 2.2 and Sec. 2.3) for map element learning, and adopts a structured encoder-decoder Transformer architecture to efficiently predict map elements (see Sec. 2.4).

2.2 HIERARCHICAL MATCHING

MapTR parallelly infers a fixed-size set of N map elements in a single pass, following the end-to-end paradigm of DETR (Carion et al., 2020). N is set to be larger than the typical number of map elements in a scene. Let's denote the set of N predicted map elements by $\hat{Y} = \{\hat{y}_i\}_{i=0}^{N-1}$. The set of ground-truth (GT) map elements is padded with \emptyset (no object) to form a set with size N , denoted by $Y = \{y_i\}_{i=0}^{N-1}$. $y_i = (c_i, V_i, \Gamma_i)$, where c_i , V_i and Γ_i are respectively the target class label, point set and permutation group of GT map element y_i . $\hat{y}_i = (\hat{p}_i, \hat{V}_i)$, where \hat{p}_i and \hat{V}_i are respectively the predicted classification score and predicted point set. To achieve structured map element modeling and learning, MapTR introduces hierarchical bipartite matching, *i.e.*, performing instance-level matching and point-level matching in order.

Instance-level Matching. First, we need to find an optimal instance-level label assignment $\hat{\pi}$ between predicted map elements $\{\hat{y}_i\}$ and GT map elements $\{y_i\}$. $\hat{\pi}$ is a permutation of N elements ($\hat{\pi} \in \Pi_N$) with the lowest instance-level matching cost:

$$\hat{\pi} = \arg \min_{\pi \in \Pi_N} \sum_{i=0}^{N-1} \mathcal{L}_{\text{ins_match}}(\hat{y}_{\pi(i)}, y_i). \quad (3)$$

$\mathcal{L}_{\text{ins_match}}(\hat{y}_{\pi(i)}, y_i)$ is a pair-wise matching cost between prediction $\hat{y}_{\pi(i)}$ and GT y_i , which considers both the class label of map element and the position of point set:

$$\mathcal{L}_{\text{ins_match}}(\hat{y}_{\pi(i)}, y_i) = \mathcal{L}_{\text{Focal}}(\hat{p}_{\pi(i)}, c_i) + \mathcal{L}_{\text{position}}(\hat{V}_{\pi(i)}, V_i). \quad (4)$$

$\mathcal{L}_{\text{Focal}}(\hat{p}_{\pi(i)}, c_i)$ is the class matching cost term, defined as the Focal Loss (Lin et al., 2017) between predicted classification score $\hat{p}_{\pi(i)}$ and target class label c_i . $\mathcal{L}_{\text{position}}(\hat{V}_{\pi(i)}, V_i)$ is the position matching cost term, which reflects the position correlation between the predicted point set $\hat{V}_{\pi(i)}$ and the GT point set V_i (refer to Sec. 3.2 for more details). Hungarian algorithm is utilized to find the optimal instance-level assignment $\hat{\pi}$ following DETR.

Point-level Matching. After instance-level matching, each predicted map element $\hat{y}_{\hat{\pi}(i)}$ is assigned with a GT map element y_i . Then for each predicted instance assigned with positive labels ($c_i \neq \emptyset$), we perform point-level matching to find an optimal point2point assignment $\hat{\gamma} \in \Gamma$ between predicted point set $\hat{V}_{\hat{\pi}(i)}$ and GT point set V_i . $\hat{\gamma}$ is selected among the predefined permutation group Γ and with the lowest point-level matching cost:

$$\hat{\gamma} = \arg \min_{\gamma \in \Gamma} \sum_{j=0}^{N_v-1} D_{\text{Manhattan}}(\hat{v}_j, v_{\gamma(j)}). \quad (5)$$

$D_{\text{Manhattan}}(\hat{v}_j, v_{\gamma(j)})$ is the Manhattan distance between the j -th point of the predicted point set \hat{V} and the $\gamma(j)$ -th point of the GT point set V .

2.3 END-TO-END TRAINING

MapTR is trained based on the optimal instance-level and point-level assignment ($\hat{\pi}$ and $\{\hat{\gamma}_i\}$). The loss function is mainly composed of three parts, classification loss, point2point loss and direction loss, *i.e.*,

$$\mathcal{L} = \lambda \mathcal{L}_{\text{cls}} + \alpha \mathcal{L}_{\text{p2p}} + \beta \mathcal{L}_{\text{dir}}, \quad (6)$$

where λ , α and β are the weights for balancing different loss terms.

Classification Loss. According to the instance-level optimal matching result $\hat{\pi}$, each predicted map element is assigned with a class label (or 'no object' \emptyset). The classification loss is a Focal Loss term formulated as:

$$\mathcal{L}_{\text{cls}} = \sum_{i=0}^{N-1} \mathcal{L}_{\text{Focal}}(\hat{p}_{\hat{\pi}(i)}, c_i). \quad (7)$$

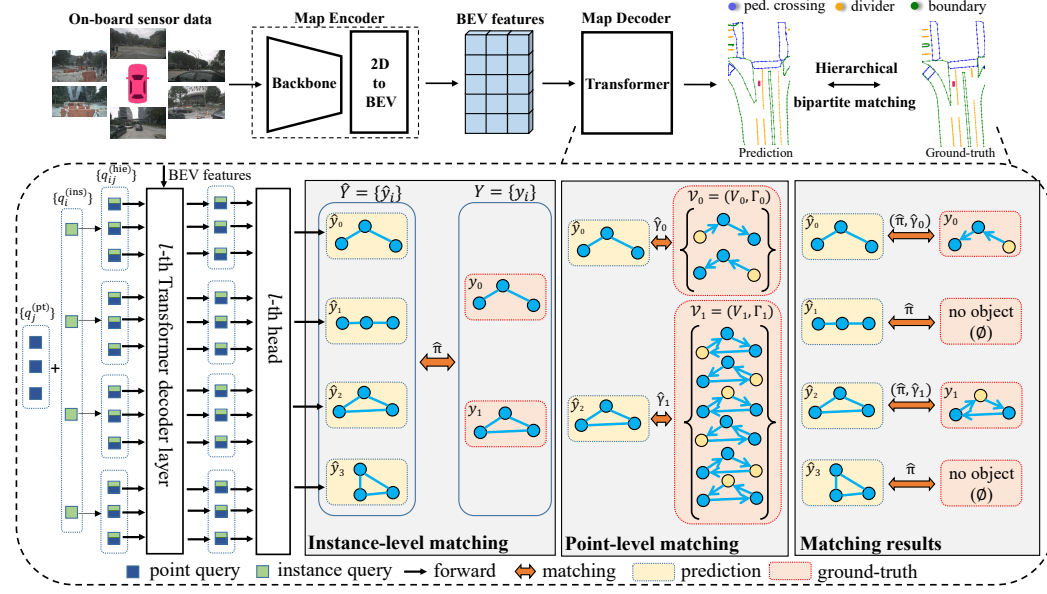


Figure 4. The overall architecture of MapTR. MapTR adopts an encoder-decoder paradigm. The map encoder transforms sensor input to a unified BEV representation. The map decoder adopts a hierarchical query embedding scheme to explicitly encode map elements and performs hierarchical matching based on the permutation-based modeling. MapTR is fully end-to-end. The pipeline is highly structured, compact and efficient.

Point2point Loss. Point2point loss aims at restricting the position of each predicted point. For each GT instance with index i , according to the point-level optimal matching result $\hat{\gamma}_i$, each predicted point $\hat{v}_{\hat{\pi}(i),j}$ is assigned with a GT point $v_{i,\hat{\gamma}_i(j)}$. The point2point loss is defined as the Manhattan distance computed between each assigned point pair:

$$\mathcal{L}_{p2p} = \sum_{i=0}^{N-1} \mathbb{1}_{\{c_i \neq \emptyset\}} \sum_{j=0}^{N_v-1} D_{\text{Manhattan}}(\hat{v}_{\hat{\pi}(i),j}, v_{i,\hat{\gamma}_i(j)}). \quad (8)$$

Edge Direction Loss. Point2point loss only restricts the node point of polyline and polygon, not considering the edge (the connecting line between adjacent points). For accurately representing map elements, the direction of the edge is important. Thus, we further design edge direction loss to restrict the geometrical shape at the higher edge level. Specifically, we consider the cosine similarity of the paired predicted edge $\hat{e}_{\hat{\pi}(i),j}$ and GT edge $e_{i,\hat{\gamma}_i(j)}$:

$$\begin{aligned} \mathcal{L}_{\text{dir}} &= - \sum_{i=0}^{N-1} \mathbb{1}_{\{c_i \neq \emptyset\}} \sum_{j=0}^{N_v-1} \text{cosine_similarity}(\hat{e}_{\hat{\pi}(i),j}, e_{i,\hat{\gamma}_i(j)}), \\ \hat{e}_{\hat{\pi}(i),j} &= \hat{v}_{\hat{\pi}(i),j} - \hat{v}_{\hat{\pi}(i),(j+1) \bmod N_v}, \\ e_{i,\hat{\gamma}_i(j)} &= v_{i,\hat{\gamma}_i(j)} - v_{i,\hat{\gamma}_i(j+1) \bmod N_v}. \end{aligned} \quad (9)$$

2.4 ARCHITECTURE

MapTR adopts an encoder-decoder paradigm. The overall architecture is depicted in Fig. 4.

Input Modality. In this work, we focus on camera-based MapTR. MapTR is compatible with various kinds of onboard sensors (camera, LiDAR, and RADAR). Extending MapTR to multi-modality data is straightforward and trivial, which will be presented in future work. And thanks to the rational permutation-based modeling, even with only camera input, MapTR significantly outperforms other methods with multi-modality input.

Map Encoder. The encoder of MapTR extracts features from original sensor data and transforms sensor features into a unified feature representation, *i.e.*, BEV representation. For camera-based MapTR, given multi-view images $\mathcal{I} = \{I_1, \dots, I_K\}$, we leverage a conventional backbone to generate multi-view feature maps $\mathcal{F} = \{F_1, \dots, F_K\}$. Then 2D image features \mathcal{F} are transformed to BEV features $\mathcal{B} \in \mathbb{R}^{H \times W \times C}$. By default, we adopt GKT (Chen et al., 2022b) as the basic 2D-to-BEV transformation module, considering its easy-to-deploy property and high efficiency. MapTR is compatible with other transformation methods and maintains stable performance, *e.g.*, CVT (Zhou & Krähenbühl, 2022), LSS (Phillion & Fidler, 2020; Liu et al., 2022c; Li et al., 2022b; Huang et al., 2021), Deformable Attention (Li et al., 2022c; Zhu et al., 2021) and IPM (Mallot et al., 1991). Ablation studies are presented in Tab. 3.

Map Decoder. We adopt a hierarchical query embedding scheme to explicitly encode each map element. Specifically, we define a set of instance-level queries $\{q_i^{(\text{ins})}\}_{i=0}^{N_v-1}$ and a set of point-level queries $\{q_j^{(\text{pt})}\}_{j=0}^{N_v-1}$ shared by all instances. Each map element (with index i) corresponds to a set of hierarchical queries $\{q_{ij}^{(\text{hie})}\}_{j=0}^{N_v-1}$. The hierarchical query of j -th point of i -th map element is formulated as:

$$q_{ij}^{(\text{hie})} = q_i^{(\text{ins})} + q_j^{(\text{pt})}. \quad (10)$$

The map decoder contains several cascaded decoder layers which update the hierarchical queries iteratively. In each decoder layer, we adopt MHSA to make hierarchical queries exchange information with each other (both inter-instance and intra-instance). We then adopt Deformable Attention (Zhu et al., 2021) to make hierarchical queries interact with BEV features, inspired by BEVFormer (Li et al., 2022c). Each query $q_{ij}^{(\text{hie})}$ predicts the 2-dimension normalized BEV coordinate (x_{ij}, y_{ij}) of the reference point p_{ij} . We then sample BEV features around the reference points and update queries.

Map elements are usually with irregular shapes and require long-range context. Each map element corresponds to a set of reference points $\{p_{ij}\}_{j=0}^{N_v-1}$ with flexible and dynamic distribution. The reference points $\{p_{ij}\}_{j=0}^{N_v-1}$ can adapt to the arbitrary shape of map element and capture informative context for map element learning.

The prediction head of MapTR is simple, consisting of a classification branch and a point regression branch. The classification branch predicts instance class score. The point regression branch predicts the positions of the point sets \hat{V} . For each map element, it outputs a $2N_v$ -dimension vector, which represents normalized BEV coordinates of the N_v points.

3 EXPERIMENTS

Dataset and Metric. We evaluate MapTR on the popular nuScenes (Caesar et al., 2020) dataset, which contains 1000 scenes of roughly 20s duration each. Key samples are annotated at 2Hz. Each sample has RGB images from 6 cameras and covers 360° horizontal FOV of the ego-vehicle. Following the previous methods (Li et al., 2022a; Liu et al., 2022a), three kinds of map elements are chosen for fair evaluation – pedestrian crossing, lane divider, and road boundary. The perception ranges are $[-15.0m, 15.0m]$ for the X -axis and $[-30.0m, 30.0m]$ for the Y -axis. And we adopt average precision (AP) to evaluate the map construction quality. Chamfer distance D_{Chamfer} is used to determine whether the prediction and GT are matched or not. We calculate the AP_τ under several D_{Chamfer} thresholds ($\tau \in T, T = \{0.5, 1.0, 1.5\}$), and then average across all thresholds as the final AP metric:

$$\text{AP} = \frac{1}{|T|} \sum_{\tau \in T} \text{AP}_\tau. \quad (11)$$

Implementation Details. MapTR is trained with 8 NVIDIA GeForce RTX 3090 GPUs. We adopt AdamW (Loshchilov & Hutter, 2019) optimizer and cosine annealing schedule. The initial learning rate is set to $6e^{-4}$. For MapTR-tiny, we adopt ResNet50 (He et al., 2016) as the backbone. We set the size of each BEV grid to $0.3m$ and stack 6 transformer decoder layers. We train MapTR-tiny

with a total batch size of 32 (containing 6 view images). All ablation studies are based on MapTR-tiny trained with 24 epochs. MapTR-nano is designed for real-time application. We adopt ResNet18 as the backbone. We set the size of each BEV grid to $0.75m$ and stack 2 transformer decoder layers. And we train MapTR-nano with a total batch size of 192. As for hyper-parameters of loss weight, λ is set to 2, α is set to 5, and β is set to $5e^{-3}$. All source code and models will be available to the public at <https://github.com/hustvl/MapTR>.

3.1 COMPARISONS WITH STATE-OF-THE-ART METHODS

In Tab. 1, we compare MapTR with state-of-the-art methods. MapTR-nano runs at real-time inference speed (25.1 FPS) on RTX 3090, $8\times$ faster than the existing state-of-the-art camera-based method (VectorMapNet-C) while achieving 3.3 higher mAP. MapTR-tiny significantly outperforms the existing state-of-the-art multi-modality method (VectorMapNet-C&L) by 13.5 mAP while being faster.

Method	Modality	Backbone	Epochs	AP_{ped}	$AP_{divider}$	$AP_{boundary}$	mAP	FPS
HDMaNet	C	Effi-B0	30	14.4	21.7	33.0	23.0	0.8
HDMaNet	L	PointPillars	30	10.4	24.1	37.9	24.1	1.0
HDMaNet	C & L	Effi-B0 & PointPillars	30	16.3	29.6	46.7	31.0	0.5
VectorMapNet	C	R50	110	36.1	47.3	39.3	40.9	2.9
VectorMapNet	L	PointPillars	110	25.7	37.6	38.6	34.0	-
VectorMapNet	C & L	R50 & PointPillars	110	37.6	50.5	47.5	45.2	-
MapTR-nano	C	R18	110	38.8	47.6	46.1	44.2	25.1
MapTR-tiny	C	R50	24	46.3	51.5	53.1	50.3	11.2
MapTR-tiny	C	R50	110	56.2	59.8	60.1	58.7	11.2

Table 1. Comparisons with state-of-the-art methods (Liu et al., 2022a; Li et al., 2022a). “C” and “L” respectively denotes camera and LiDAR. “Effi-B0” and “PointPillars” respectively correspond to Tan & Le (2019) and Lang et al. (2019). The APs of other methods are taken from the paper of VectorMapNet. The FPS of VectorMapNet-C is provided by its authors and measured on RTX 3090. Other FPSs are measured on the same machine with RTX 3090. “-” means that the corresponding results are not available. Even with only camera input, MapTR-tiny significantly outperforms multi-modality counterparts (+13.5 mAP). MapTR-nano achieves SOTA camera-based performance and runs at 25.1 FPS, realizing real-time vectorized map construction for the first time.

3.2 ABLATION STUDY

Modeling Method. In Tab. 2, we provide ablation experiments to validate the effectiveness of the proposed permutation-based modeling. Compared with vanilla modeling method which imposes a unique permutation to the point set, permutation-based modeling solves the definition ambiguity of map element and brings an improvement of 5.9 mAP. For pedestrian crossing, the improvement even reaches 11.9 AP, proving the superiority in modeling polygon elements.

Modeling method	AP_{ped}	$AP_{divider}$	$AP_{boundary}$	mAP
Fixed-order V^F w/ ambiguity	34.4	48.1	50.7	44.4
Permutation-based (V, Γ) w/o ambiguity	46.3	51.5	53.1	50.3

Table 2. Ablations about modeling method. Vanilla modeling method imposes a unique permutation to the point set, leading to definition ambiguity. MapTR introduces permutation-based modeling to avoid the ambiguity, which eases learning and significantly improves performance (+5.9 mAP).

2D-to-BEV Transformation. In Tab. 3, we ablate on the 2D-to-BEV transformation methods. We use an optimized implementation of LSS (Liu et al., 2022c). And for fair comparison with IPM and LSS, GKT and Deformable Attention both adopt one-layer configuration. The ablations show MapTR is compatible with various 2D-to-BEV methods and achieves stable performance. We adopt GKT as the default configuration of MapTR, considering its easy-to-deploy property and high efficiency.

Method	mAP	FPS	Param.
IPM (Mallot et al., 1991)	46.2	11.7	35.7M
LSS (Liu et al., 2022c; Phillion & Fidler, 2020)	49.5	10.0	37.1M
Deform. Atten. (Li et al., 2022c; Zhu et al., 2021)	49.7	11.2	36.0M
GKT (Chen et al., 2022b)	50.3	11.2	35.9M

Table 3. Ablations about 2D-to-BEV transformation methods. MapTR is compatible with various 2D-to-BEV methods and achieves stable performance.

Point Number. Ablations about the number of points for modeling each map element are presented in Tab. 4. Too few points can not describe the complex geometrical shape of the map element. Too many points affect the efficiency. We adopt 20 points as the default setting of MapTR.

Pt. num.	AP _{ped}	AP _{divider}	AP _{boundary}	mAP	FPS
10	42.5	51.3	50.1	48.0	12.3
20	46.3	51.5	53.1	50.3	11.2
40	44.7	52.4	52.9	50.0	10.8

Table 4. Ablations about the number of points for modeling each map element.

Decoder Layer Number. Ablations about the layer number of map decoder are presented in Tab. 5. The map construction performance improves with more layers, but gets saturated when the layer number reaches 6.

Layer num.	AP _{ped}	AP _{divider}	AP _{boundary}	mAP	FPS
1	20.8	30.2	36.3	29.1	15.2
2	36.0	43.1	48.0	42.4	14.2
3	38.2	44.1	49.5	44.0	13.5
6	46.3	51.5	53.1	50.3	11.2
8	39.6	51.9	51.2	47.6	10.6

Table 5. Ablations about the number of decoder.

Position Matching Cost. As mentioned in Sec. 2.2, we adopt the position matching cost term $\mathcal{L}_{\text{position}}(\hat{V}_{\pi(i)}, V_i)$ in instance-level matching, for reflecting the position correlation between the predicted point set $\hat{V}_{\pi(i)}$ and the GT point set V_i . In Tab. 6, we compare two kinds of cost design. *i.e.*, Chamfer distance cost and point2point cost. Point2point cost is similar to the point-level matching cost. Specifically, we find the best point2point assignment, and sum the Manhattan distance of all point pairs as the position matching cost of two point sets. The experiments show point2point cost is better than Chamfer distance cost.

Edge Direction Loss. Ablations about the weight of edge direction loss are presented in Tab. 7. $\beta = 0$ means that we do not use edge direction loss. $\beta = 5e^{-3}$ corresponds to appropriate supervision and is adopted as the default setting.

3.3 QUALITATIVE VISUALIZATION

We show the predicted vectorized HD map results of complex and various driving scenes in Fig. 1. MapTR maintains stable and impressive results. More qualitative results are provided in Appendix.

4 RELATED WORK

HD Map Construction. HD Map is vital for autonomous vehicles. Recently, with the development of 2D-to-BEV methods (Ma et al., 2022), HD map construction is formulated as a segmentation problem based on surround-view image data captured by onboard cameras. Chen et al. (2022b); Zhou & Krähenbühl (2022); Hu et al. (2021); Li et al. (2022c); Phillion & Fidler (2020);

Position matching cost	AP_{ped}	$AP_{divider}$	$AP_{boundary}$	mAP
Chamfer distance cost	40.3	53.8	48.5	47.5
Point2point cost	46.3	51.5	53.1	50.3

Table 6. Ablations about the position matching cost term.

β	AP_{ped}	$AP_{divider}$	$AP_{boundary}$	mAP
0	41.4	51.3	51.9	48.2
$3e^{-3}$	44.8	50.4	52.1	49.1
$5e^{-3}$	46.3	51.5	53.1	50.3
$1e^{-2}$	41.9	50.9	52.0	48.3

Table 7. Ablations about the weight β of edge direction loss.

Liu et al. (2022b) generate rasterized map by performing BEV semantic segmentation. To build vectorized HD map, HDMaNet (Li et al., 2022a) groups pixel-wise semantic segmentation results with heuristic and time-consuming post-processing to generate instances. To eliminate the post-processing, VectorMapNet (Liu et al., 2022a) adopts a two-stage pipeline. The first stage utilizes set prediction method to detect coarse keypoints and the second stage utilizes sequence generation method to sequentially predict the next point of the map element. Different from VectorMapNet, MapTR introduces novel and unified modeling for map element, solving the definition ambiguity and easing learning. And MapTR builds a structured and parallel one-stage framework with much higher efficiency.

Lane Detection. Lane detection can be viewed as a sub task of HD map construction, which focuses on detecting lane elements in the road scenes. Since most datasets of lane detection only provide single view annotations and focus on open-shape elements, related methods are restricted to single view. LaneATT (Tabelini et al., 2021) utilizes anchor-based deep lane detection model to achieve good trade-off between accuracy and efficiency. LSTR (Liu et al., 2021a) adopts the Transformer architecture to directly output parameters of a lane shape model. GANet (Wang et al., 2022) formulates lane detection as a keypoint estimation and association problem and takes a bottom-up design. Feng et al. (2022) proposes parametric Bezier curve-based method for lane detection. Instead of detecting lane in the 2D image coordinate, Garnett et al. (2019) proposes 3D-LaneNet which performs 3D lane detection in BEV. STSU (Can et al., 2021) represents lanes as a directed graph in BEV coordinates and adopts curve-based Bezier method to predict lanes from monocular camera image. Persformer (Chen et al., 2022a) provides better BEV feature representation and optimizes anchor design to unify 2D and 3D lane detection simultaneously. Instead of only detecting lanes in the limited single view, MapTR can perceive various kinds of map elements of 360° horizontal FOV, with a unified modeling and learning framework.

Contour-based Instance Segmentation. Another line of work related to MapTR is contour-based 2D instance segmentation (Zhu et al., 2022; Xie et al., 2020; Xu et al., 2019; Liu et al., 2021b). These methods reformulate 2D instance segmentation as object contour prediction task, and estimate the image coordinates of the contour vertices. CurveGCN (Ling et al., 2019) utilizes Graph Convolution Networks to predict polygonal boundaries. Deepsnake (Peng et al., 2020) proposes a two-stage contour evolution process and designs circular convolution to exploit the features on the contour. BoundaryFormer (Lazarow et al., 2022) introduces polygon-based differentiable rasterization to directly predict object’s boundary. Unlike these works of 2D instance segmentation based on single-view image, MapTR is tailored for HD map construction in the driving scenario. Based on the prior knowledge of 3D scene, MapTR abstracts and models various kinds of map elements in a unified manner, *i.e.*, a point set with a group of equivalent permutations. And a structured framework is introduced for efficient map element learning.

5 CONCLUSION

MapTR is a structured end-to-end framework for efficient online vectorized HD map construction, based on the proposed permutation-based modeling. Abundant visualization results prove that

MapTR works well in various driving scenarios and is of great practical value. We hope MapTR can serve as a basic module of self-driving system and boost the development of downstream tasks (*e.g.*, motion prediction and planning).

ACKNOWLEDGMENT

We would like to thank Yicheng Liu for his guidance on evaluation and constructive discussions.

REFERENCES

- Holger Caesar, Varun Bankiti, Alex H Lang, Sourabh Vora, Venice Erin Liong, Qiang Xu, Anush Krishnan, Yu Pan, Giancarlo Baldan, and Oscar Beijbom. nuscenes: A multimodal dataset for autonomous driving. In *CVPR*, 2020.
- Yigit Baran Can, Alexander Liniger, Danda Pani Paudel, and Luc Van Gool. Structured bird’s-eye-view traffic scene understanding from onboard images. In *ICCV*, 2021.
- Nicolas Carion, Francisco Massa, Gabriel Synnaeve, Nicolas Usunier, Alexander Kirillov, and Sergey Zagoruyko. End-to-end object detection with transformers. In *ECCV*, 2020.
- Li Chen, Chonghao Sima, Yang Li, Zehan Zheng, Jiajie Xu, Xiangwei Geng, Hongyang Li, Conghui He, Jianping Shi, Yu Qiao, and Junchi Yan. Persformer: 3d lane detection via perspective transformer and the openlane benchmark. In *ECCV*, 2022a.
- Shaoyu Chen, Tianheng Cheng, Xinggang Wang, Wenming Meng, Qian Zhang, and Wenyu Liu. Efficient and robust 2d-to-bev representation learning via geometry-guided kernel transformer. *arXiv preprint arXiv:2206.04584*, 2022b.
- Zhengyang Feng, Shaohua Guo, Xin Tan, Ke Xu, Min Wang, and Lizhuang Ma. Rethinking efficient lane detection via curve modeling. In *CVPR*, 2022.
- Noa Garnett, Rafi Cohen, Tomer Pe’er, Roei Lahav, and Dan Levi. 3d-lanenet: end-to-end 3d multiple lane detection. In *ICCV*, 2019.
- Kaiming He, Xiangyu Zhang, Shaoqing Ren, and Jian Sun. Deep residual learning for image recognition. In *CVPR*, 2016.
- Anthony Hu, Zak Murez, Nikhil Mohan, Sofía Dudas, Jeffrey Hawke, Vijay Badrinarayanan, Roberto Cipolla, and Alex Kendall. FIERY: Future instance segmentation in bird’s-eye view from surround monocular cameras. In *ICCV*, 2021.
- Junjie Huang, Guan Huang, Zheng Zhu, Ye Yun, and Dalong Du. Bevdet: High-performance multi-camera 3d object detection in bird-eye-view. *arXiv preprint arXiv:2112.11790*, 2021.
- Alex H. Lang, Sourabh Vora, Holger Caesar, Lubing Zhou, Jiong Yang, and Oscar Beijbom. Pointpillars: Fast encoders for object detection from point clouds. In *CVPR*, 2019.
- Justin Lazarow, Weijian Xu, and Zhuowen Tu. Instance segmentation with mask-supervised polygonal boundary transformers. In *CVPR*, 2022.
- Qi Li, Yue Wang, Yilun Wang, and Hang Zhao. Hdmapnet: An online hd map construction and evaluation framework. In *ICRA*, 2022a.
- Yinhao Li, Zheng Ge, Guanyi Yu, Jinrong Yang, Zengran Wang, Yukang Shi, Jianjian Sun, and Zeming Li. Bevdepth: Acquisition of reliable depth for multi-view 3d object detection. *arXiv preprint arXiv:2206.10092*, 2022b.
- Zhiqi Li, Wenhao Wang, Hongyang Li, Enze Xie, Chonghao Sima, Tong Lu, Yu Qiao, and Jifeng Dai. Bevformer: Learning bird’s-eye-view representation from multi-camera images via spatiotemporal transformers. In *ECCV*, 2022c.
- Tsung-Yi Lin, Priya Goyal, Ross B. Girshick, Kaiming He, and Piotr Dollár. Focal loss for dense object detection. In *ICCV*, 2017.

- Huan Ling, Jun Gao, Amlan Kar, Wenzheng Chen, and Sanja Fidler. Fast interactive object annotation with curve-gcn. In *CVPR*, 2019.
- Ruijin Liu, Zejian Yuan, Tie Liu, and Zhiliang Xiong. End-to-end lane shape prediction with transformers. In *WACV*, 2021a.
- Yicheng Liu, Yue Wang, Yilun Wang, and Hang Zhao. Vectormapnet: End-to-end vectorized hd map learning. *arXiv preprint arXiv:2206.08920*, 2022a.
- Zhi Liu, Shaoyu Chen, Xiaojie Guo, Xinggang Wang, Tianheng Cheng, Hongmei Zhu, Qian Zhang, Wenyu Liu, and Yi Zhang. Vision-based uneven bev representation learning with polar rasterization and surface estimation. *arXiv preprint arXiv:2207.01878*, 2022b.
- Zhijian Liu, Haotian Tang, Alexander Amini, Xingyu Yang, Huizi Mao, Daniela Rus, and Song Han. Bevfusion: Multi-task multi-sensor fusion with unified bird’s-eye view representation. *arXiv preprint arXiv:2205.13542*, 2022c.
- Zichen Liu, Jun Hao Liew, Xiangyu Chen, and Jiashi Feng. Dance: A deep attentive contour model for efficient instance segmentation. In *WACVW*, 2021b.
- Ilya Loshchilov and Frank Hutter. Decoupled weight decay regularization. In *ICLR*, 2019.
- Yuexin Ma, Tai Wang, Xuyang Bai, Huitong Yang, Yuenan Hou, Yaming Wang, Y. Qiao, Ruigang Yang, Dinesh Manocha, and Xinge Zhu. Vision-centric bev perception: A survey. *arXiv preprint arXiv:2208.02797*, 2022.
- Hanspeter A Mallot, Heinrich H Bülthoff, JJ Little, and Stefan Bohrer. Inverse perspective mapping simplifies optical flow computation and obstacle detection. *Biological cybernetics*, 1991.
- Sida Peng, Wen Jiang, Huaijin Pi, Xiuli Li, Hujun Bao, and Xiaowei Zhou. Deep snake for real-time instance segmentation. In *CVPR*, 2020.
- Jonah Philion and Sanja Fidler. Lift, splat, shoot: Encoding images from arbitrary camera rigs by implicitly unprojecting to 3d. In *ECCV*, 2020.
- Tixiao Shan and Brendan Englot. Lego-loam: Lightweight and ground-optimized lidar odometry and mapping on variable terrain. In *IROS*, 2018.
- Tixiao Shan, Brendan J. Englot, Drew Meyers, Wei Wang, Carlo Ratti, and Daniela Rus. LIO-SAM: tightly-coupled lidar inertial odometry via smoothing and mapping. In *IROS*, 2020.
- Lucas Tabelini, Rodrigo Berriel, Thiago M Paixao, Claudine Badue, Alberto F De Souza, and Thiago Oliveira-Santos. Keep your eyes on the lane: Real-time attention-guided lane detection. In *CVPR*, 2021.
- Mingxing Tan and Quoc V. Le. Efficientnet: Rethinking model scaling for convolutional neural networks. In *ICML*, 2019.
- Jinsheng Wang, Yinchao Ma, Shaofei Huang, Tianrui Hui, Fei Wang, Chen Qian, and Tianzhu Zhang. A keypoint-based global association network for lane detection. In *CVPR*, 2022.
- Enze Xie, Peize Sun, Xiaoge Song, Wenhai Wang, Xuebo Liu, Ding Liang, Chunhua Shen, and Ping Luo. Polarmask: Single shot instance segmentation with polar representation. In *CVPR*, 2020.
- Wenqiang Xu, Haiyang Wang, Fubo Qi, and Cewu Lu. Explicit shape encoding for real-time instance segmentation. In *ICCV*, 2019.
- Ji Zhang and Sanjiv Singh. LOAM: lidar odometry and mapping in real-time. In *Robotics: Science and Systems X, University of California*, 2014.
- Brady Zhou and Philipp Krähenbühl. Cross-view transformers for real-time map-view semantic segmentation. In *CVPR*, 2022.

Chenming Zhu, Xuanye Zhang, Yanran Li, Liangdong Qiu, Kai Han, and Xiaoguang Han. Sharp-contour: A contour-based boundary refinement approach for efficient and accurate instance segmentation. In *CVPR*, 2022.

Xizhou Zhu, Weijie Su, Lewei Lu, Bin Li, Xiaogang Wang, and Jifeng Dai. Deformable DETR: deformable transformers for end-to-end object detection. In *ICLR*, 2021.